IEEE Access
Multidisciplinary | Rapid Review | Open Access Journal

Received September 18, 2018, accepted October 8, 2018, date of publication October 18, 2018,
date of current version December 18, 2018.

Digital Object Identifier 10.1109/ACCESS.2018.2876645

Onboard Battery Chargers for Plug-in Electric Vehicles With Dual Functional Circuit for Low-Voltage Battery Charging and Active Power Decoupling

HOANG VU NGUYEN, (Student Member, IEEE), DINH-DU TO, AND DONG-CHOON LEE, (Senior Member, IEEE)
Department of Electrical Engineering, Yeungnam University, Gyeongsan 38541, South Korea

Corresponding author: Dong-Choon Lee (dclee@yu.ac.kr)

This work was supported by the National Research Foundation of Korea, funded by the South Korean Government, under Grant NRF-2017R1A2A2A05069629.

ABSTRACT This paper proposes a single-phase onboard battery charger (OBC) for plug-in electric vehicles, where the low-voltage (LV) battery charging circuit is utilized for an active power decoupling function. The OBC is operated in three different modes by sharing the transformer, switches, and capacitors. For a grid-to-vehicle mode or a vehicle-to-grid mode, the LV battery charging circuit serves as an active filter to eliminate the low-frequency power ripple at the DC link. Thus, the small film capacitors can be employed instead of large capacitors at the DC link. For the third operating mode, where the LV battery is charged from the HV battery, the isolation is provided by the dual active bridge (DAB) DC-DC converter. Since some components in the proposed OBC are used in common, the size and cost of the OBC can be reduced significantly. The simulation and experimental results have verified the validity of the proposed system.

INDEX TERMS Active power decoupling, electric vehicles, onboard battery charger, single-phase chargers.

I. INTRODUCTION

Nowadays, with the advent of more stringent regulations related to emission, global warning, and resource constraints, electric vehicles (EVs) have attracted an increasing attention from vehicle manufacturers, governments, and consumers[1]–[5]. In plug-in EVs, the batteries are usually charged from the grid by the onboard battery charger (OBC). In general, there are two kinds of usages for batteries in the EVs. One is the high-voltage (HV) battery for traction motor drives and the other is the low-voltage (LV) battery for auxiliary power supplies feeding the loads such as lighting and signaling circuits, entertainments, automatic seats, and other electronic devices. The LV battery is charged from the HV battery by the auxiliary charger since alternators are not used, differently from the conventional vehicles equipped with an internal combustion engine.

In single-phase HV battery chargers, there is an inherent ripple power component in the DC link that is fluctuated at double the grid frequency, which causes the DC-link ripple voltage. To smoothen this low-frequency ripple power, the large capacitors are usually needed. However, since the electrolytic capacitors are not desirable in EV applications due to its short lifetime, it is necessary to replace them by the reliable film capacitor, of which size should be optimized. For this, the ripple power of the DC link needs to be diverted to other energy storage elements which allow large fluctuations in the voltage [6]. As a result, the DC-link capacitor can be much reduced in size and weight.

Recently, a number of active power decoupling circuits have been proposed to reduce the ripple power at the DC link [7]–[14]. The basic concept of this method is to utilize auxiliary circuits to absorb the ripple power, which leads to the increase in system complexity, cost, and additional losses. Another method for reducing the DC-link capacitance in the single-phase OBC is to charge the HV battery with the same frequency of current as that of ripple power [6], [15], [16]. In this way, the second-order ripple power flows into the HV battery, not the DC-link capacitor at all, so a small film capacitor can be adopted. However, the sinusoidal charging current causes a relatively higher heating in the battery [17].

More recently, some multifunctional OBCs have been proposed [18], [19], which operate in three different modes; grid-to-vehicle (G2V), vehicle-to-grid (V2G), and HV-battery-to-LV-battery (H2L). In the G2V mode, the HV battery is charged from the power grid and in the V2G mode the HV battery supplies the grid. For the H2L mode, the LV battery is charged from the HV battery. Meanwhile, much attention has been paid to reducing the volume and weight of the OBC, for which some devices are utilized in common to reduce the number of the circuit components [18]–[21]. However, a reduction of capacitor size has not been investigated in these works. In [22] and [23], an integration of functions of active power filter and LV battery charger has been introduced to reduce the overall size of the converter, where the circuit is operated only in a unidirectional power flow. Also, the capacitor in the active power decoupling (APD) circuit is not fully utilized, so, the decoupling performance is limited.

In this paper, a single-phase OBC for plug-in EVs with a dual functional circuit is proposed, which can operate not only in three different modes but also in an active power decoupling function [24]. When the charger is operated in G2V or V2G modes, the LV battery charging circuit functions as an active filter to eliminate the low-frequency ripple power at the DC link. As a result, small film capacitors can be employed instead of large electrolytic types at the DC-link. With the proposed LV battery charger with the active power decoupling function, the size and cost of the single-phase OBC can be reduced significantly. The validity of the proposed system is verified by simulation and experimental results.

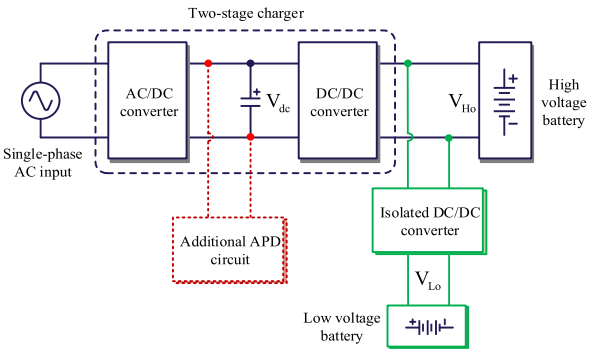

FIGURE 1. The conventional two-stage onboard charger with additional active power decoupling circuit.

II. PROPOSED ONBOARD BATTERY CHARGERS WITH DUAL FUNCTIONAL CIRCUIT

Figure 1 shows the conventional two-stage dual-voltage charging system which consists of an HV battery charger and an LV battery charger [25]. Also, the additional APD circuit is used to absorb the ripple power. In the two-stage charger, an AC/DC power factor correction (PFC) boost converter is usually combined with either non-isolated or isolated DC/DC converter. The main function of the second- stage DC/DC converter is to regulate the voltage and current of the HV battery. The advantages of the two-stage topology are that it provides high power factor, sinusoidal grid current, and ripple-less charging current [6].

A. CIRCUIT CONFIGURATION OF PROPOSED ONBOARD BATTERY CHARGER

Figure 2 shows a circuit configuration of the proposed battery charger with dual functional. The first stage is a full-bridge AC-DC converter, the second one is a dual active bridge (DAB) DC-DC converter, and the last one is a dual functional circuit (DFC) for LV battery charging and active power decoupling.

For G2V or V2G modes, the SW_1 is closed and the SW_2 is connected to point "a". In these modes, the HV battery is charged from the grid or releases power back to the grid, where the DFC works as an active power decoupling (APD) circuit which absorbs the inherent ripple power in the single-phase system. Next, for H2L mode, the SW_1 is open and the SW_2 is connected to point "b". In this operation, the LV battery is charged by the DFC from the HV battery, where two identical capacitors (C_{dc1} and C_{dc2}) are the output filter of the DAB converter.

B. PROPOSED LV BATTERY CHARGER WITH ACTIVE POWER DECOUPLING FUNCTION

In order to achieve the APD function, the connection of the LV charger is moved to the DC link of the HV charger, rather than being connected directly to the HV battery. For an LV battery charger, the DAB converter and DFC are operated as a two-stage DC-DC converter. For an APD circuit, on the other hand, an auxiliary inductor, L_r, is added. Then, the symmetrical half-bridge circuit with two identical capacitors, $C_{dc1} = C_{dc2} = C_f$, and a small inductor, L_r, is operated as an active power filter. The relay, SW_2, is used for switching between APD function and LV battery charging.

Furthermore, if the switching devices of the DFC are integrated with those of the single-phase full-bridge AC-DC converter, a three-phase intelligent power module (IPM) can be employed, which results in a compact design of hardware.

III. CONTROL METHOD FOR PROPOSED BATTERY CHARGERS

A. G2V AND V2G MODES

When the HV charger is operated in G2V or V2G modes, the DFC acts as an APD circuit, as shown in Figure 3. For analysis of ripple power in the single-phase system, it is assumed that the single-phase charger is operated at unity power factor and that the grid voltage, $v_s(t)$, and the grid current, $i_s(t)$ are sinusoidal, respectively, as

$$v_s(t) = \sqrt{2}V_s \sin(\omega t) \tag{1}$$

$$i_s(t) = \sqrt{2}I_s \sin(\omega t) \tag{2}$$

where V_s and I_s are the rms values of the grid voltage and current, respectively, and ω is the line angular frequency. Then, the instantaneous AC input power, $p_0(t)$, is expressed

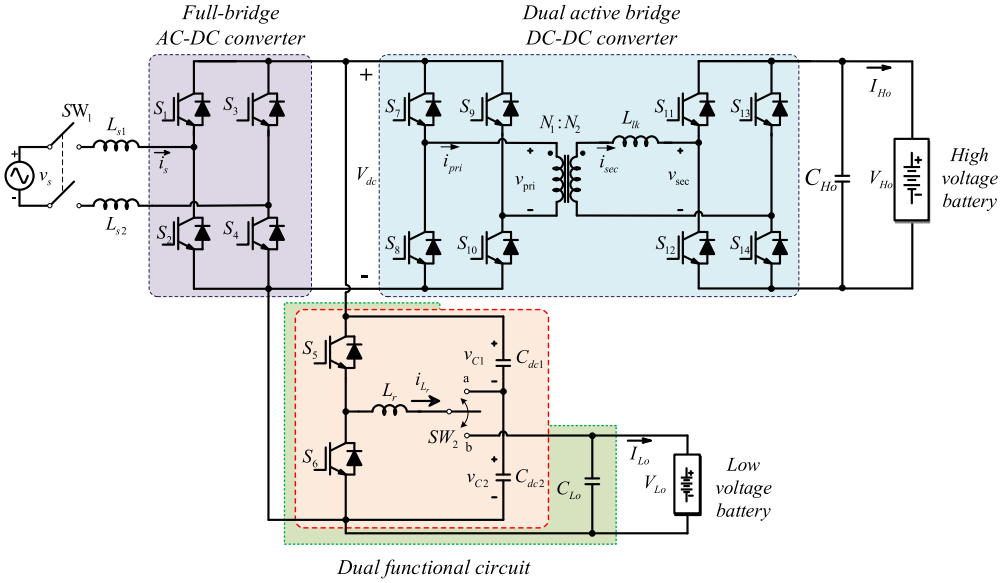

FIGURE 2. Circuit configuration of the proposed onboard battery charger.

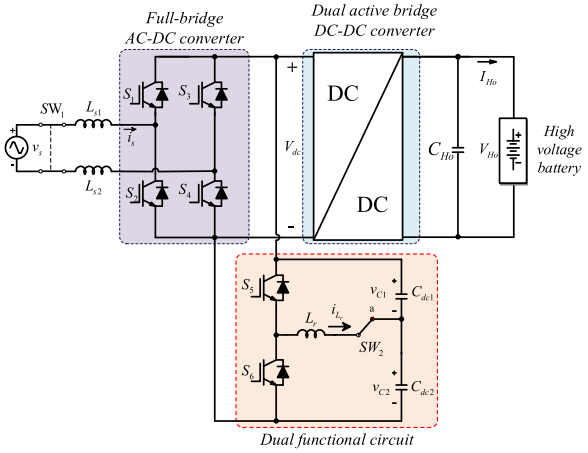

FIGURE 3. Operation of the proposed OBC in G2V and V2G mode.

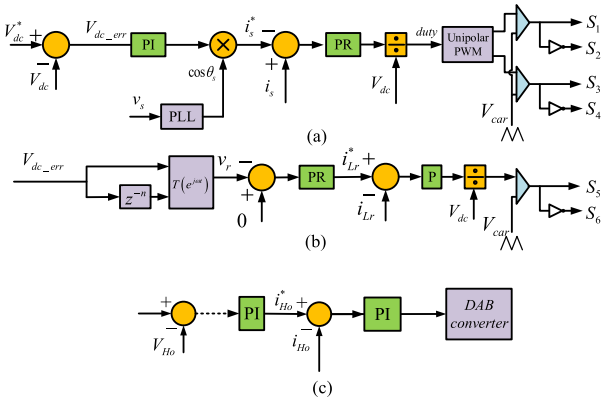

FIGURE 4. Control block diagram of the proposed battery charger in G2V mode. (a) AC-DC converter. (b) APD circuit. (c) DAB converter.

as

$$p_0(t) = v_s(t)\, i_s(t) + L_s \frac{di_s(t)}{dt} = V_s I_s - V_s I_s \cos(2\omega t) - \omega L_s I_s^2 \sin(2\omega t). \quad (3)$$

where $L_s = (2L_{s1} = 2L_{s2})$ represents the input inductance of the AC-DC converter.

The time-varying terms on the right-hand side in (3) are the ripple component to be compensated by the DFC. In order to achieve this, the upper and lower capacitor voltages, which should be controlled to be sinusoidal with an offset value that is equal to a half of the DC-link voltage, $\frac{V_{dc}}{2}$, can be expressed, respectively, as [7]

$$v_{c1}^* = \frac{V_{dc}}{2} - \sqrt{2} V_c \cos(\omega t + \varphi) \quad (4)$$

$$v_{c2}^* = \frac{V_{dc}}{2} + \sqrt{2} V_c \cos(\omega t + \varphi), \quad (5)$$

where

$$V_c = \sqrt{\frac{\sqrt{(V_s I_s)^2 + \left(\omega L_s I_s^2\right)^2}}{\omega C_f - 2\omega L_r \left(\omega C_f\right)^2}} \quad (6)$$

$$\varphi = \frac{1}{2} \arctan\left(-\frac{V_s}{\omega L_s I_s}\right). \quad (7)$$

If the control performance is ideal, the ripple power at the DC link would be canceled completely. However, it is difficult to achieve an ideal power decoupling due to the uncertainties and disturbances of the system. Therefore, a closed-loop control is applied to solve this issue instead of using (4) and (5) [26].

Figure 4 shows the control block diagram of the AC-DC converter and APD circuit in G2V mode, where the proportional-integral (PI) and proportional-resonant (PR) controllers are adopted to control the DC-link voltage and

grid current, respectively. The aim of the APD circuit is to force the ripple voltage component in the DC link to be zero. Since the input error of the DC-link voltage controller has the second-order harmonic component, it is transformed into the fundamental one, which is the same as the capacitor voltage waveform in (5), by applying the transformation matrix of

$$T(\omega t) = \begin{bmatrix} \cos(\omega t) & \sin(\omega t) \\ -\sin(\omega t) & \cos(\omega t) \end{bmatrix} \tag{8}$$

In V2G mode, the power delivered to the grid from the HV battery is controlled by the DAB converter, whereas the DC-link voltage and grid current are controlled by the full-bridge AC-DC converter.

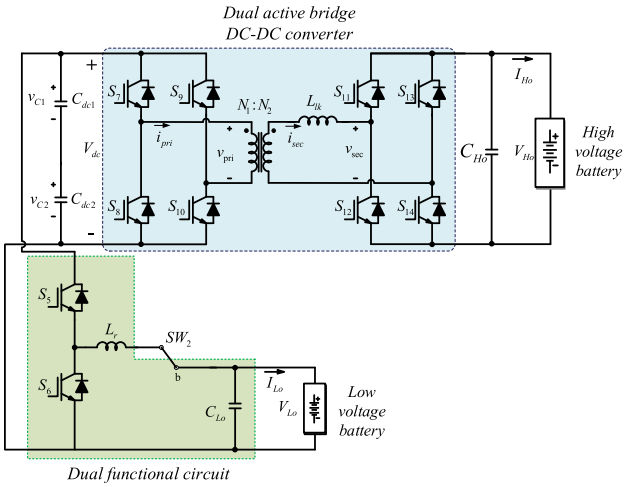

FIGURE 5. Operation of the proposed OBC in H2L mode.

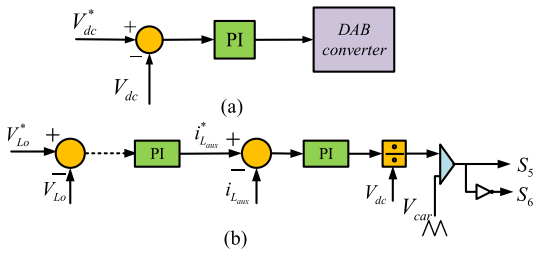

FIGURE 6. Control block diagram of the proposed battery charger in H2L mode. (a) DAB converter. (b) DFC.

B. H2L MODE FOR LV BATTERY CHARGING

When the SW_1 is OFF, the vehicle is disconnected to the grid, whereas the SW_2 is connected to terminal "b" and then the system can operate as a two-stage DC-DC converter to charge the LV battery, as shown in Figure 5. Figure 6 shows the control block diagram of the system operating in H2L mode. In this mode, the DC-link voltage is controlled by the DAB DC-DC converter, where the PI controller is adopted, as shown in Figure 6(a). For charging the LV battery, the PI controller is used to control the current of the LV battery, as shown in Figure 6(b).

IV. DESIGN CONSIDERATION

A. H2L DESIGN OF CAPACITORS AND INDUCTOR FOR APD CIRCUIT

It is assumed that the ripple power in the input inductor, L_s, and filter inductor, L_r, is neglected since its value is too low compared with that of the capacitors, C_{dc1} and C_{dc2}. Then, the ripple power of the APD circuit is highest when

$$V_c = \frac{V_{dc}}{2}. \tag{9}$$

From (6) and (9), the capacitance, C_f, of the filter capacitor is obtained as

$$C_f = \frac{4V_s I_s}{V_{dc}^2 \omega} \tag{10}$$

Here, the equivalent DC-link capacitance, C_{eq}, is defined as

$$C_{eq} = \frac{C_f}{2} = \frac{2V_s I_s}{\omega V_{dc}^2} = \frac{2P_{in}}{\omega V_{dc}^2}, \tag{11}$$

where P_{in} is the input power.

For instance, for a 60-Hz system with the DC-link voltage of 350V, the required equivalent capacitance per input power is about 43 μF/kW. However, in a practical condition, the highest voltage in the capacitors is a little lower than $V_{dc}/2$. Also, the ripple power in L_s and L_r needs to be considered to determine the capacitance. Finally, for the 3.3-kW system, the equivalent DC-link capacitance is selected as 150μF and $C_f (= C_{dc1} = C_{dc2}) = 300\mu$F.

On the other hand, for the conventional full-bridge AC-DC converter, the DC capacitance is given by [9]

$$C = \frac{P_{in}}{\omega V_{dc} \triangle V_{dc}}. \tag{12}$$

If the specified peak-to-peak ripple voltage, $\triangle V_{dc}$, is set to 7 V, the required capacitance is about 3.5 mF.

Also, to select the filter inductor, L_r, of the APD circuit, a cancelation coefficient, α, is defined as [27]

$$\alpha = \omega^2 L_r C_f, \tag{13}$$

from which

$$L_r = \frac{\alpha}{\omega^2 C_f}. \tag{14}$$

In this work, the cancelation coefficient is chosen as 0.075. Then, the inductance of the filter inductor is computed as 1.5 mH.

B. H2L DESIGN OF LEAKAGE INDUCTANCE FOR DUAL ACTIVE BRIDGE CONVERTER

The DAB converter has a capability of bidirectional power transfers, which is accomplished by controlling the phase-shift ratio between primary voltage, v_{pri}, and secondary voltage, v_{sec}. The power of the DAB converter is given as [28]

$$P_D = \frac{V_1 V_2}{2nf_{sw}L_{lk}} d(1-d) \tag{15}$$

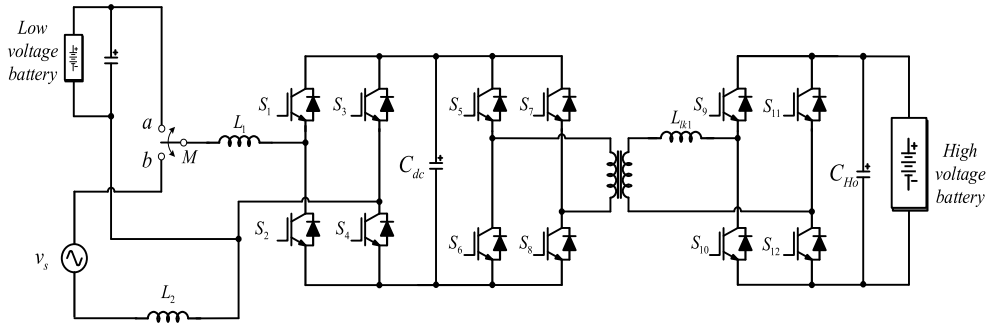

FIGURE 7. Circuit configurations of OBC and LV battery charger in [20].

where V_1 and V_2 are the input and the output voltages of the DAB, n is the turn ratio of the transformer, f_{sw} is the switching frequency, d is the phase-shift ratio, and L_{lk} is the leakage inductance.

The leakage inductance is determined based on minimized current stresses to improve the efficiency of the DAB converter. The current stresses on the DAB converter are a function of the maximum phase-shift ratio, the leakage inductance, and the maximum voltage conversion ratio, $M_{\max}$, where the voltage conversion ratio is defined as

$$M = n\frac{V_2}{V_1} \tag{16}$$

If the DAB converter is operated under minimum current stresses, the optimal phase-shift ratio is chosen as [29]

$$d_{opt} = \frac{1 - M_{\max} + \sqrt{M_{\max}^2 - 1}}{2} \tag{17}$$

From (15) an (17), the leakage inductance of the DAB converter is obtained as

$$L_{lk} = \frac{V_1 V_2 d_{opt}\left(1 - d_{opt}\right)}{2 f_{sw} n P_D}. \tag{18}$$

For a 3.3-kW system, the leakage inductance is calculated as about 100μH.

V. COMPARATIVE STUDY OF EFFICIENCY, COST, AND VOLUME OF THE SYSTEM

In this section, the efficiency, cost, and volume of the proposed battery charger are evaluated and compared with those of existing circuit shown in Figure 7 since it also provides the multi-task by sharing the transformer [20]. For evaluation, the system specifications are assumed as follows:

1) HV battery voltage: 250 V and LV battery voltage: 24 V.

2) Output power capacity of the HV battery in G2V and V2G modes: 3.3-kW and 1.5-kW, respectively.

3) LV battery in a charging mode: 1 kW.

4) Turn ratio of the transformer in the separated OBC and the proposed OBC: $N_1/N_2 = 1.4$.

5) Turn ratio of the transformer in the LV charger of the separated OBC: $N_1/N_2 = 0.2$.

6) Capacitor types: Metallized polypropylene film capacitors.

A. EFFICIENCY

The efficiency of the proposed OBC in three different modes is shown in Figure 8, for which the thermal module of the PSIM software was utilized [30]. For G2V mode, the efficiencies of the AC/DC converter and the DAB converter are about 95.7% and 96.8%, respectively, at full load condition and then the overall efficiency is about 92.6%, which are shown in Figure 8(a). For V2G mode, the overall efficiency is about 91.8% at the full-load condition, as shown in Figure 8(b). During V2G mode, the overall efficiency of the AC/DC converter is estimated between 90.8% and 95.3%. In this mode, the efficiency of the DAB converter varies between 91.4% and 96.3%. Figure 8(c) shows the efficiency of the proposed charger operating in H2L mode. The overall efficiency is ranged between 77.7% and 89.24%. Figure 8(d) shows the efficiencies for the existing topologies in [20], [21], and [31] when operating in G2V mode. Due to the additional auxiliary circuit, the efficiency of the proposed converter is lowered by 1.7% compared with that of the existing charger [20] at full load condition.

B. COST AND VOLUME

The proposed charger is able to perform multitasks by sharing switches and inductors in a single board. By virtue of this, the charger can be designed in a smaller size.

A cost comparison between the existing topology and the proposed circuit is performed, where the costs of the switches, gating drivers, inductors, and capacitors of the converter are taken into account, but some circuit components such as sensors, heat sink, windings, and batteries are excluded.

Table 1 lists the count of devices and the cost of the two topologies. Due to the decrease of capacitance at the DC-link capacitor and the transformer, the overall cost of the proposed circuit is reduced by about 53.4% compared with the existing one, as shown in Figure 9(a).

In addition, the evaluation of the volume of the main components in the existing and proposed circuits is summarized in Table 2. The volume of the circuits is calculated from their dimensions provided in the datasheets [32]–[35]. For the proposed topology, the overall volume of the main components is decreased by 70.2% compared with that of the existing one [20], as shown in Figure 9(b).

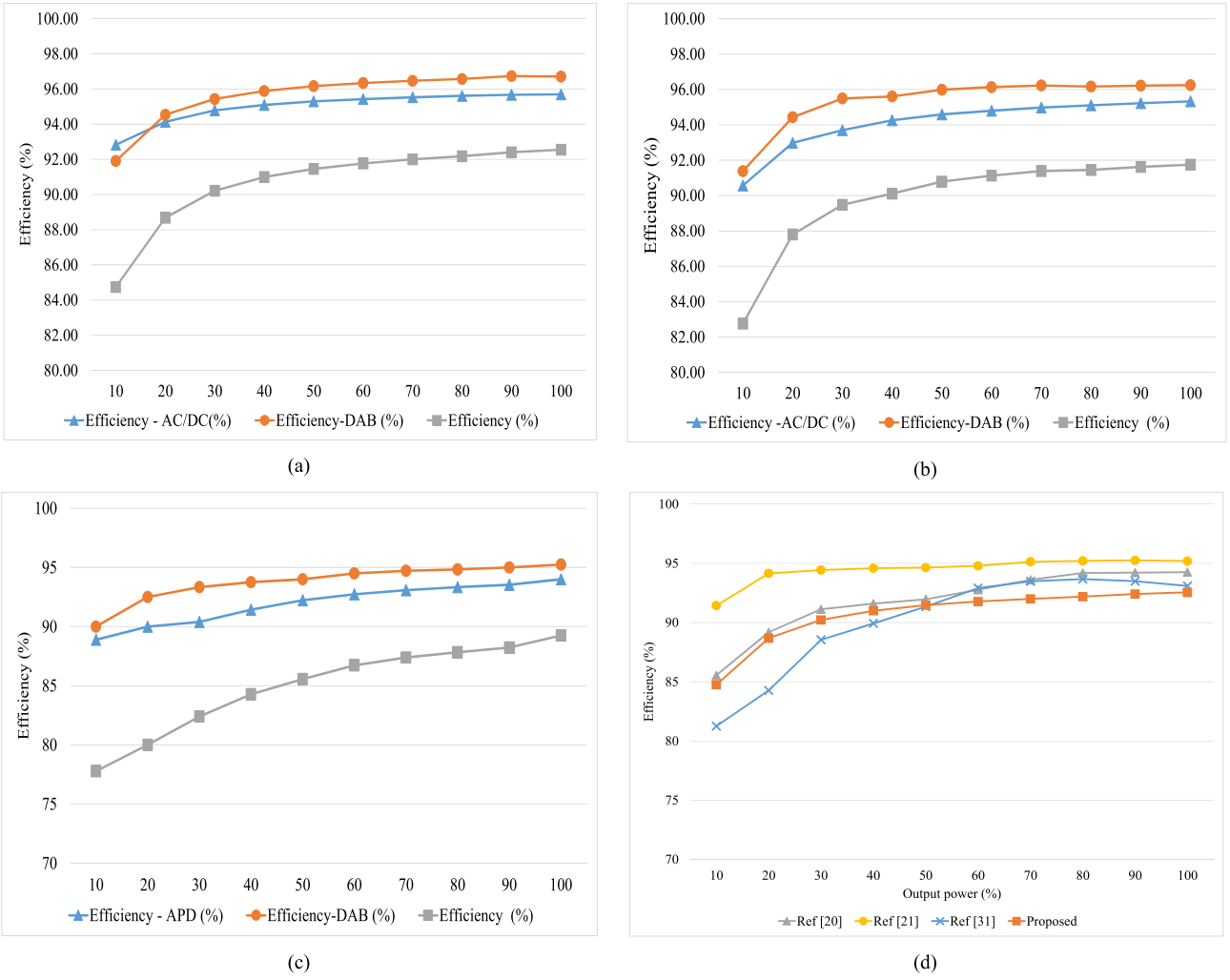

FIGURE 8. The efficiency of the proposed OBC in three different modes. (a) G2V mode. (b) V2G mode. (c) H2L mode. (d) G2V mode for different topologies.

TABLE 1. Cost comparison of existing and proposed topologies.

Devices	Topology in [20]			Proposed Topology		
	Type	no.	Cost (USD)	Type	no.	Cost (USD)
IGBTs	SK45GB063	4	103.68	SK45GB063	6	155.52
	SKM 75GB063D	2	86.72	SKM 75GB063D	1	43.36
Inductor core	PC47EE60-Z	2	28.42	PC47EE60-Z	1	14.21
				PC47EE50-Z	2	24.26
Transformer core	PC47EE60-Z	1	14.21	PC47EE60-Z	1	14.21
Capacitors	MKP1848720454Y5	17	1518.1	MKP1848720454Y5	2	89.3
	MKP1848710454Y5	1	40.3	MKP1848710454Y5	2	40.3
Gate driver	SKYPER 32 R	6	460.8	SKYPER 32 R	7	537.6
Relay	898-1CH-D-R1	1	2.44	898-1CH-D-R1	1	2.44
Summation			**2,254.67**			**1,050.80**

VI. SIMULATION RESULTS

To test the operation of the proposed circuit, the PSIM simulation has been performed for a 3.3-kW system. The system parameters are listed in Table 3.

Figure 10 shows the simulation results of the proposed battery charger operating in G2V mode, where the DFC works as an APC circuit. It is seen in Figure 10(a) that the DC-link ripple voltage is about 0.2%, where the average value of the DC-link voltage is 350 V. The grid current and voltage are shown in Figure 10(b), where the grid current is controlled to be sinusoidal at unity power factor. Figure 10(c) shows the upper and lower capacitor voltages which are sinusoidal.

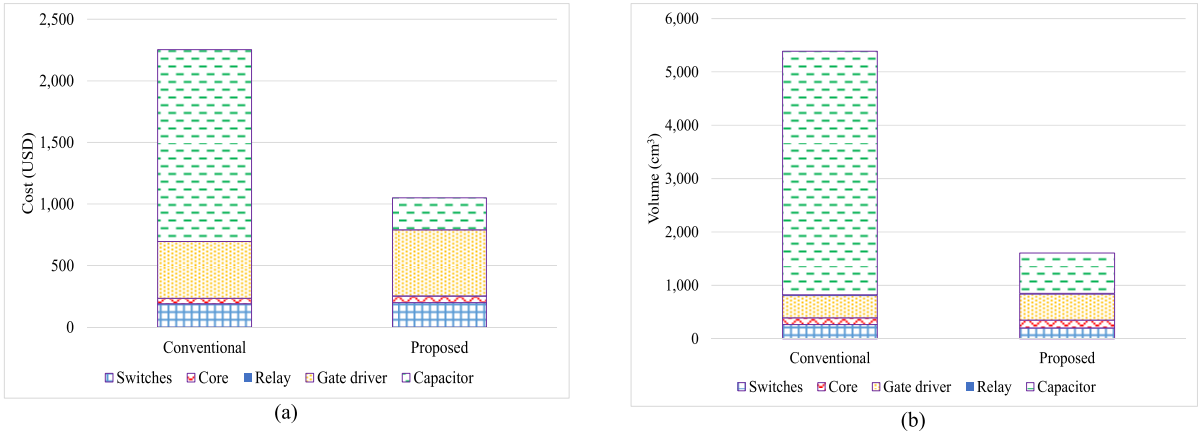

FIGURE 9. Comparison of cost and volume. (a) Cost. (b) Volume.

TABLE 2. Comparison of volumes of existing and proposed topologies.

Devices	Topology in [20]			Proposed Topology		
	Type	no.	Volume (mm^3)	Type	no.	Volume (mm^3)
Switches	SK45GB063	4	69,990	SK45GB063	6	104,986
	SKM 75GB063D	2	194,956	SKM 75GB063D	1	97,478
Inductor core	PC47EE60-Z	2	83,491	PC47EE60-Z	1	41,745
				PC47EE50-Z	2	62,196
Transformer core	PC47EE60-Z	1	41,746	PC47EE60-Z	1	41,745
Capacitors	MKP1848720454Y5	17	4,447,625	MKP1848720454Y5	2	523,250
	MKP1848710454Y5	1	116,438	MKP1848710454Y5	2	232,875
Gate driver	SKYPER 32 R	6	415,872	SKYPER 32 R	7	485.184
Relay	898-1CH-D-R1	1	16.641	898-1CH-D-R1	1	16.641
Summation			**5,386,759**			**1,606,101**

TABLE 3. Parameters of ev charging system.

Parameters	**Value**
Power rating of HV charger	3.3 kW
Power rating of LV charger	1 kW
DC-link voltage	350 V
Input voltage	220 V (RMS) 60 Hz
C_f	300 μF
L_r	1.5 mH
R_{Ho}, R_{Lo}	19 Ω, 0.5 Ω
Transformer turn ratio	1.75:1
HV battery voltage	250 V
LV battery voltage	24 V
C_{aux}	200 μF
C_{Ho}	200 μF
Switching frequency	10 kHz
L_{s1}, L_{s2}	1.5 mH
L_k	100 μH

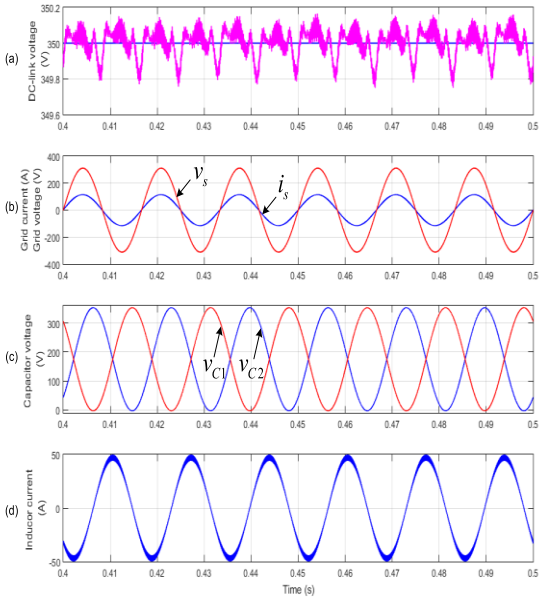

FIGURE 10. Control of battery charger in G2V mode. (a) DC-link voltage. (b) Grid current and voltage. (c) Capacitor voltages. (d) Inductor current.

They match well with the results of the theoretical analysis. Figure 10(d) shows the inductor current, of which peak value is about 50A.

Figure 11 shows the control performance of the DAB converter at a constant-current charging condition. The currents and voltages of the DAB converter are shown in

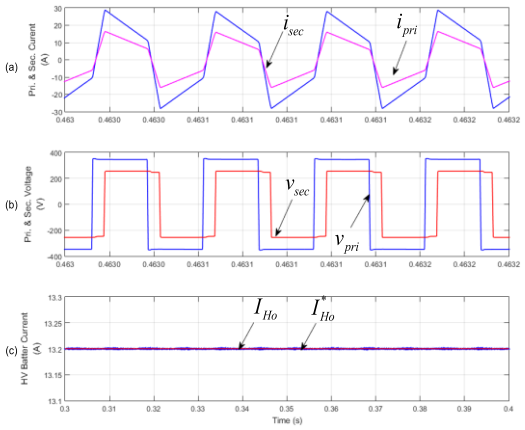

FIGURE 11. Control performance of DAB converter at constant-current charging profile. (a) Primary and secondary currents. (b) Primary and secondary voltages. (c) HV battery current.

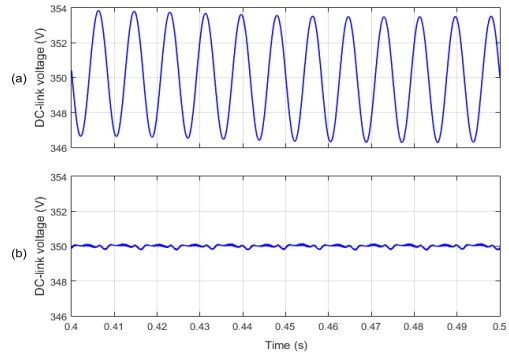

FIGURE 12. Comparison of DC-link voltage ripples. (a) Conventional method with 3500-μF DC-link capacitors. (b) Proposed method with 150-μF DC-link capacitors.

Figure 11(a) and (b), respectively. In this operation mode, since the power flows from the primary side to the secondary one, the primary voltage lags the secondary one. Figure 11(c) shows the HV battery charging current, which is well regulated at its reference. Since the main objective of this research work is to integrate the LV battery charger and APD circuit in a multifunctional system, the detailed charging algorithm of the HV battery is not described in this manuscript [36], [37].

Figure 12(a) and (b) show the comparison of the DC-link voltage ripples for the conventional scheme with large capacitors and the proposed APD method with small capacitors, respectively. In the conventional topology, a 3500-μF capacitor is needed to reduce the DC-link ripple voltage below 2% of the average value. However, the proposed method needs at most 150-μF capacitors.

The operation of the proposed charger in V2G mode is shown in Figure 13. In this case, the DAB converter is used to control the power, which is delivered from the battery to the grid, as shown in Figure 13(a). Figure 13(b) shows the DC-link voltage, which is well controlled with 0.2% ripple of the average value. The grid current is controlled to be sinusoidal for unity power factor, as shown in Figure 13(c). The currents and voltages of the DAB converter are shown in Figure 13(d) and (e), respectively. Since the power flows from

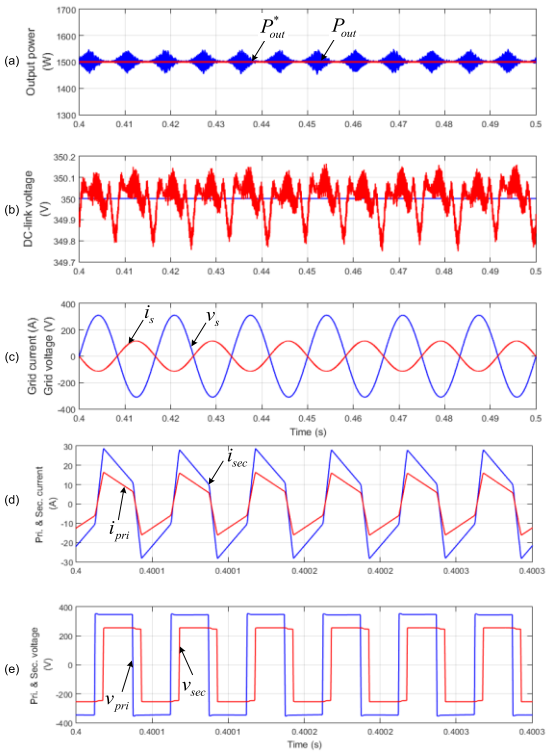

FIGURE 13. Control of battery charger in V2G mode. (a) Power. (b) DC-link voltage. (c) Grid current and voltage. (d) Primary and secondary currents. (e) Primary and secondary voltages.

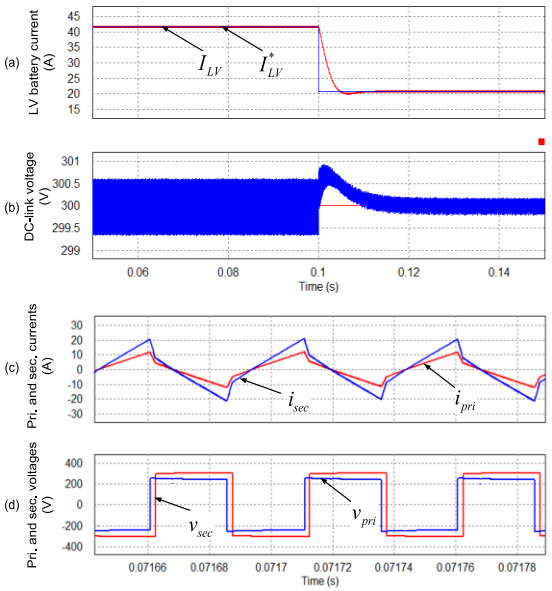

FIGURE 14. Control of battery charger in H2L mode. (a) LV battery current. (b) DC-link voltage. (c) Primary and secondary currents. (d) Primary and secondary voltages.

the secondary side to the primary one, the secondary voltage lags the primary one.

Figure 14 shows the control performance in the case of the H2L operating mode. Figure 14(a) shows the LV battery current, which is well controlled at its reference. The DC-link voltage is well controlled at 300 V, as shown in Figure 14(b),

where it is lowered than that of G2V or V2G modes to reduce the current stress of the switching devices. The currents and voltages of the DAB converter are shown in Figure 14(c) and (d), respectively.

VII. EXPERIMENTAL RESULTS

To verify the effectiveness of the proposed circuit, a prototype has been built at the laboratory. The system parameters are listed in Table 4. A 32-bit DSP chip (TMS320F28335) was used as the main controller, where the Xilinx FPGA device is employed to generate a switching frequency of 10 kHz.

TABLE 4. Parameters of ev charging system.

Parameters	Values
Power rating of HV charger	1 kW
Power rating of LV charger	200 W
DC-link voltage	250 V
Grid voltage	110 V RMS, 60 Hz
C_f	200 µF
L_r	1.5 mH
R_{Ho}, R_{Lo}	5 Ω, 2.5 Ω
Transformer turn ratio	6.25:1
HV battery voltage	75 V
LV battery voltage	24 V
C_{aux}	200 µF
C_{Ho}	200 µF
Switching frequency	10 kHz
L_{s1}, L_{s2}	1 mH
L_{lk}	80 µH

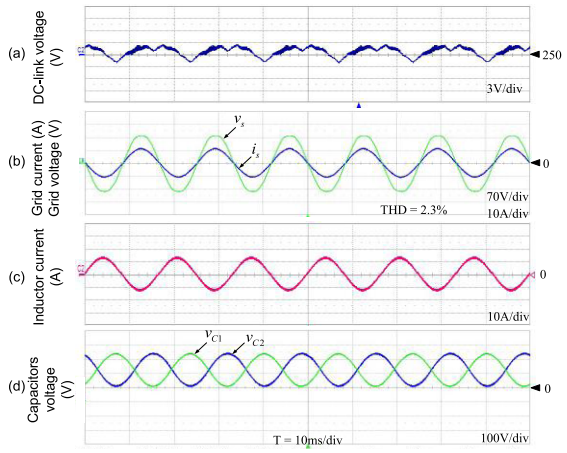

FIGURE 15. Control of battery charger in G2V mode. (a) DC-link voltage. (b) Input current and voltage. (c) Inductor current. (d) Capacitor voltages.

Figure 15 shows the operating performance of the proposed battery charger in G2V mode, where the DFC works as an APC circuit. It is seen from Figure 15(a) that the DC-link voltage ripple is about 2%. The grid current and voltage are shown in Figure 15(b), where the grid current is controlled to be sinusoidal at unity power factor. The inductor current is shown in Figure 15(c), of which peak value is about 22A. Figure 15(d) shows the upper and lower capacitor voltages which are sinusoidal.

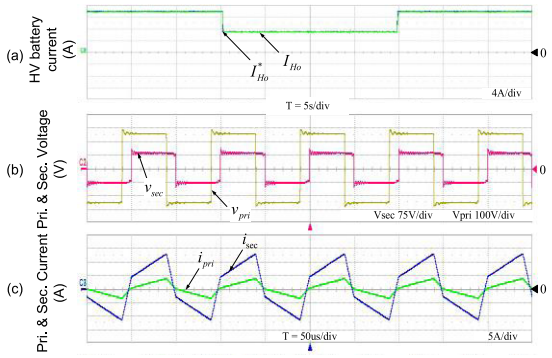

FIGURE 16. Control performance of battery charger in G2V mode. (a) Charging current. (b) Primary and secondary voltages. (c) Primary and secondary currents.

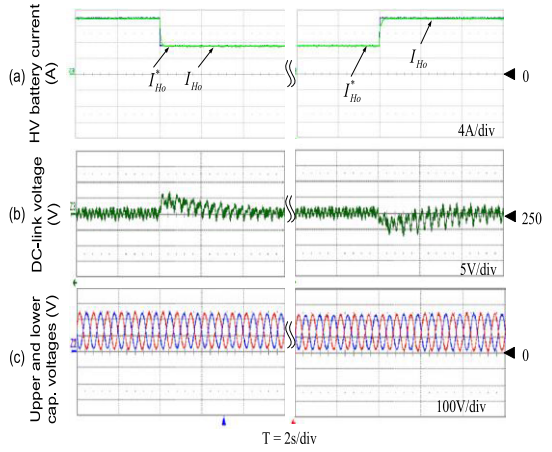

FIGURE 17. Control performance of battery charger in G2V mode. (a) HV battery current. (b) DC-link voltage. (c) Capacitor voltages.

Figure 16 shows the control performance of the DAB converter in a constant-current charging operation. Figure 16(a) shows the HV battery current, which is well regulated at its reference. Figure 16(b) shows the primary and secondary voltages of the transformer, where the voltage level step-downs from 250 V to 75 V. Figure 16(c) shows the primary and secondary currents, from which the power is known to transfer from the primary to the secondary. Figure 17 shows the control performance of the battery charger system at the same load change as in Figure 16. It is seen that the DC-link voltage variation is kept below 5V. The capacitor voltage waveforms are sinusoidal.

Figure 18 shows the operating performance of the battery charger in V2G mode where the proposed OBC works as a DC-AC inverter. For load variations, the DC-link voltage is well controlled with 2% ripple components. The grid current is controlled to be sinusoidal at unity power factor. The total harmonic distortion of the output voltage is about 2.5%. It is obvious that the experimental results are in a close match with simulation ones of in Figure 13.

When the battery charger is operated in H2L mode, the experimental results of the proposed OBC are shown

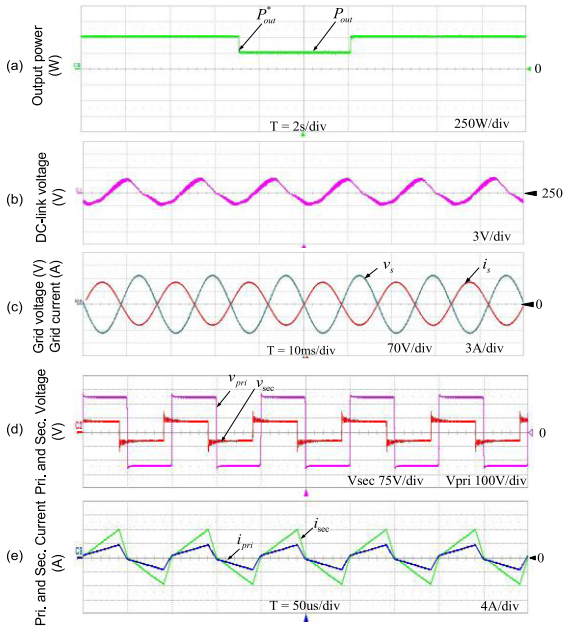

FIGURE 18. Control of battery charger in V2G mode. (a) Power. (b) DC-link voltage. (c) Grid current and voltage. (d) Primary and secondary voltages. (e) Primary and secondary currents.

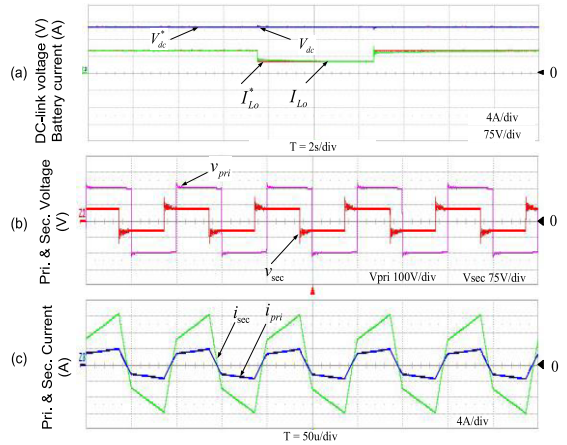

FIGURE 19. Control of battery charger in H2L mode. (a) LV battery current and DC-link voltage. (b) Primary and secondary voltages. (c) Primary and secondary currents.

in Figure 19, which are also similar to simulation ones shown in Figure 14.

VIII. CONCLUSION

This paper has proposed a new single-phase onboard battery charger for plug-in EVs without the bulky DC-link capacitors, which is able to function for three tasks: G2V, V2G, and H2L modes. The proposed OBC utilizes the LV battery charger as an active power filter to eliminate the second-order ripple power when the EVs are connected to the grid. By adding an inductor on the primary side of the LV charger, the converter can achieve the APC function without adding additional switches, heat sinks, and gate drive circuits. In addition, when the charger operates in H2L mode, the isolation between the HV and LV batteries is provided by the transformer of the DAB DC-DC converter. As a result, for a 3.3-kW HV battery charger, the volume and cost can be decreased by 70.2% and 53.4%, based on the main components, compared with the conventional circuit, respectively. The effectiveness of the proposed charger has been verified by the experimental result for a 1-kW OBC system.

REFERENCES

[1] C. C. Chan, A. Bouscayrol, and K. Chen, "Electric, hybrid, and fuel-cell vehicles: Architectures and modeling," *IEEE Trans. Veh. Technol.*, vol. 59, no. 2, pp. 589–598, Feb. 2010.

[2] Q. Qian, W. Sun, T. Zhang, and S. Lu, "A voltage-fed single-stage PFC full-bridge converter with asymmetric phase-shifted control for battery chargers," *J. Power Electron.*, vol. 17, no. 1, pp. 31–40, Jan. 2017.

[3] M. Yilmaz and P. T. Krein, "Review of battery charger topologies, charging power levels, and infrastructure for plug-in electric and hybrid vehicles," *IEEE Trans. Power Electron.*, vol. 28, no. 5, pp. 2151–2169, May 2013.

[4] S. Haghbin, S. Lundmark, M. Alakula, and O. Carlson, "An isolated high-power integrated charger in electrified-vehicle applications," *IEEE Trans. Veh. Technol.*, vol. 60, no. 9, pp. 4115–4126, Nov. 2011.

[5] S.-W. Choi, Y.-J. Kim, I.-O. Lee, and J.-Y. Lee, "Isolated PFC converter based on an ADAB structure with harmonic modulation for EV chargers," *J. Power Electron.*, vol. 18, no. 2, pp. 383–394, Mar. 2018.

[6] K.-M. Yoo, K.-D. Kim, and J.-Y. Lee, "Single- and three-phase PHEV onboard battery charger using small link capacitor," *IEEE Trans. Ind. Electron.*, vol. 60, no. 8, pp. 3136–3144, Aug. 2013.

[7] Y. Tang, F. Blaabjerg, P. C. Loh, C. Jin, and P. Wang, "Decoupling of fluctuating power in single-phase systems through a symmetrical half-bridge circuit," *IEEE Trans. Power Electron.*, vol. 30, no. 4, pp. 1855–1865, Apr. 2015.

[8] Y. Sun, Y. Liu, M. Su, W. Xiong, and J. Yang, "Review of active power decoupling topologies in single-phase systems," *IEEE Trans. Power Electron.*, vol. 31, no. 7, pp. 4778–4794, Jul. 2016.

[9] R. Chen, Y. Liu, and F. Z. Peng, "DC capacitor-less inverter for single-phase power conversion with minimum voltage and current stress," *IEEE Trans. Power Electron.*, vol. 30, no. 10, pp. 5499–5507, Oct. 2015.

[10] M. A. Vitorino, R. Wang, M. B. de Rossiter Corrêa, and D. Boroyevich, "Compensation of DC-link oscillation in single-phase-to-single-phase VSC/CSC and power density comparison," *IEEE Trans. Ind. Appl.*, vol. 50, no. 3, pp. 2021–2028, May/Jun. 2014.

[11] H. V. Nguyen, Y.-C. Jeung, and D.-C. Lee, "Battery charger with small DC-link capacitors for G2V applications," in *Proc. IEEE Int. Conf. Sustain. Energy Technol. (ICSET)*, Nov. 2016, pp. 315–319.

[12] R. Wang *et al.*, "A high power density single-phase PWM rectifier with active ripple energy storage," *IEEE Trans. Power Electron.*, vol. 26, no. 5, pp. 1430–1443, May 2011.

[13] Y. Yang, X. Ruan, L. Zhang, J. He, and Z. Ye, "Feed-forward scheme for an electrolytic capacitor-less ac/dc LED driver to reduce output current ripple," *IEEE Trans. Power Electron.*, vol. 29, no. 10, pp. 5508–5517, Oct. 2014.

[14] L.-R. Chen, S.-L. Wu, D.-T. Shieh, and T.-R. Chen, "Sinusoidal-ripple-current charging strategy and optimal charging frequency study for li-ion batteries," *IEEE Trans. Ind. Electron.*, vol. 60, no. 1, pp. 88–97, Jan. 2013.

[15] S. Li, J. Deng, and C. C. Mi, "Single-stage resonant battery charger with inherent power factor correction for electric vehicles," *IEEE Trans. Veh. Technol.*, vol. 62, no. 9, pp. 4336–4344, Nov. 2013.

[16] L. Xue, Z. Shen, D. Boroyevich, P. Mattavelli, and D. Diaz, "Dual active bridge-based battery charger for plug-in hybrid electric vehicle with charging current containing low frequency ripple," *IEEE Trans. Power Electron.*, vol. 30, no. 12, pp. 7299–7307, Dec. 2015.

[17] A. J. Ruddell *et al.*, "Analysis of battery current microcycles in autonomous renewable energy systems," *J. Power Sour.*, vol. 112, pp. 531–546, Nov. 2002.

[18] Y.-J. Lee, A. Khaligh, and A. Emadi, "Advanced integrated bidirectional AC/DC and DC/DC converter for plug-in hybrid electric vehicles," *IEEE Trans. Veh. Technol.*, vol. 58, no. 8, pp. 3970–3980, Oct. 2009.

[19] S. Dusmez and A. Khaligh, "A compact and integrated multifunctional power electronic interface for plug-in electric vehicles," *IEEE Trans. Power Electron.*, vol. 28, no. 12, pp. 5690–5701, Dec. 2013.

[20] S. Kim and F.-S. Kang, "Multifunctional onboard battery charger for plug-in electric vehicles," *IEEE Trans. Ind. Electron.*, vol. 62, no. 6, pp. 3460–3472, Jun. 2014.
[21] J. G. Pinto, V. Monteiro, H. Gonçalves, and J. L. Afonso, "Onboard reconfigurable battery charger for electric vehicles with traction-to-auxiliary mode," *IEEE Trans. Veh. Technol.*, vol. 63, no. 3, pp. 1104–1116, Mar. 2014.
[22] R. Hou and A. Emadi, "Applied integrated active filter auxiliary power module for electrified vehicles with single-phase onboard chargers," *IEEE Trans. Power Electron.*, vol. 32, no. 3, pp. 1860–1871, Mar. 2017.
[23] R. Hou and A. Emadi, "A primary full-integrated active filter auxiliary power module in electrified vehicles with single-phase onboard chargers," *IEEE Trans. Power Electron.*, vol. 32, no. 11, pp. 8393–8405, Nov. 2017.
[24] H. V. Nguyen and D.-C. Lee, "Single-phase multifunctional onboard battery chargers with active power decoupling capability," in *Proc. IEEE Appl. Power Electron. Conf. Expo. (APEC)*, Mar. 2018, pp. 3434–3439.
[25] R. Hou and A. Emadi, "Integrated active power filter auxiliary power modules for electrified vehicle applications with single-phase on-board chargers," in *Proc. IEEE Transp. Electrific. Conf. Expo (ITEC)*, Jun. 2015, pp. 1–6.
[26] Y. Tang, Z. Qin, F. Blaabjerg, and P. C. Loh, "A dual voltage control strategy for single-phase PWM converters with power decoupling function," *IEEE Trans. Power Electron.*, vol. 30, no. 12, pp. 7060–7071, Dec. 2015.
[27] H. Li, K. Zhang, H. Zhao, S. Fan, and J. Xiong, "Active power decoupling for high-power single-phase PWM rectifiers," *IEEE Trans. Power Electron.*, vol. 28, no. 3, pp. 1308–1319, Mar. 2013.
[28] N. M. L. Tan, T. Abe, and H. Akagi, "Design and performance of a bidirectional isolated DC–DC converter for a battery energy storage system," *IEEE Trans. Power Electron.*, vol. 27, no. 3, pp. 1237–1248, Mar. 2012.
[29] F. Yazdani and M. Zolghadri, "Design of dual active bridge isolated bidirectional DC converter based on current stress optimization," in *Proc. 8th Power Electron., Drive Syst. Technol. Conf. (PEDSTC)*, Feb. 2017, pp. 247–252.
[30] H. V. Nguyen and D.-C. Lee, "Comparison of power losses in single-phase to three-phase AC/DC/AC PWM converters," in *Proc. 9th Int. Conf. Power Electron. ECCE Asia (ICPE-ECCE)*, Jun. 2015, pp. 940–945.
[31] D. S. Gautam, F. Musavi, M. Edington, W. Eberle, and W. G. Dunford, "An automotive onboard 3.3-kW battery charger for PHEV application," *IEEE Trans. Veh. Technol.*, vol. 61, no. 8, pp. 3466–3474, Oct. 2012.
[32] Mouser Electronics. *Products. Mouser Electronics*. Accessed: May 12, 2018. [Online]. Available: http://www.mouser.com/
[33] Digi-Key Electronics. *Products. Digi-Key Electronics*. Accessed: May 12, 2018. [Online]. Available: http://www.digikey.com/
[34] TDK Electronics. (2011). *Ferrite for Switching Power Supplies*. [Online]. Available: https://www.tdk.co.jp
[35] Semikron. *Products. Semikron*. Accessed: May 12, 2018. [Online]. Available: https://www.semikron.com
[36] J. C. Mukherjee and A. Gupta, "A review of charge scheduling of electric vehicles in smart grid," *IEEE Syst. J.*, vol. 9, no. 4, pp. 1541–1553, Dec. 2015.
[37] M. Yilmaz and P. T. Krein, "Review of the impact of vehicle-to-grid technologies on distribution systems and utility interfaces," *IEEE Trans. Power Electron.*, vol. 28, no. 12, pp. 5673–5689, Dec. 2013.

HOANG VU NGUYEN was born in Can Tho, Vietnam, in 1990. He received the B.S. degree in electrical engineering from Can Tho University, Can Tho, Vietnam, in 2012. He is currently pursuing the Ph.D. degree with the Department of Electrical Engineering, Yeungnam University, Gyeongsan, South Korea. In 2013, he has been a Lecturer at the Can Tho University of Technology. His current research interests include AC-DC converters, DC-AC inverters, and electric vehicle chargers.

DINH-DU TO received the B.S. degree in electrical engineering from the Ho Chi Minh City University of Technology, Ho Chi Minh City, Vietnam, in 2015. He is currently pursuing the M.S./Ph.D. degrees with the Department of Electrical Engineering, Yeungnam University, Gyeongsan, South Korea. His research interests include modeling, stability analysis, and control of DC microgrid.

DONG-CHOON LEE received the B.S., M.S., and Ph.D. degrees in electrical engineering from Seoul National University, Seoul, South Korea, in 1985, 1987, and 1993, respectively. He was a Research Engineer at Daewoo Heavy Industry, South Korea, from 1987 to 1988. He has been a faculty member at the Department of Electrical Engineering, Yeungnam University, Gyeongsan, South Korea, since 1994. He was a Visiting Scholar at the Power Quality Laboratory, Texas A&M University, College Station, TX, USA, in 1998; the Electrical Drive Center, University of Nottingham, Nottingham, U.K., in 2001; the Wisconsin Electric Machines and Power Electronics Consortium, University of Wisconsin, Madison, WI, USA, in 2004; and the FREEDM Systems Center, North Carolina State University, Raleigh, NC, USA, from 2011 to 2012. He served as the Editor-in-Chief for the *Journal of Power Electronics* of the Korean Institute of Power Electronics, from 2015 to 2017, where he is currently the Senior Vice President. His current research interests include power converter design and control, renewable energy and grid connection, AC machine drives, and power quality.